

Fast Pulse-Echo Ultrasound Imaging Employing Compressive Sensing

Martin F. Schiffner and Georg Schmitz

Chair of Medical Engineering, Ruhr-Universität Bochum, D-44801 Bochum, Germany

Copyright notice:

©2011 IEEE. Personal use of this material is permitted. Permission from IEEE must be obtained for all other uses, in any current or future media, including reprinting/republishing this material for advertising or promotional purposes, creating new collective works, for resale or redistribution to servers or lists, or reuse of any copyrighted component of this work in other works.

To be published in Proceedings of IEEE Ultrasonics Symposium (IUS), Orlando, Florida, 2011.

Fast Pulse-Echo Ultrasound Imaging Employing Compressive Sensing

Martin F. Schiffner and Georg Schmitz

Chair of Medical Engineering, Ruhr-Universität Bochum, D-44801 Bochum, Germany, Email: martin.schiffner@rub.de

Abstract—In fast pulse-echo diagnostic ultrasound imaging the acquisition time for a single image is crucial. This time depends significantly on the number of sequentially emitted sound waves. For fewer wave emissions the inverse scattering problem is increasingly ill-posed. In this contribution we establish and investigate a solution based on compressive sensing (CS). This approach accounts for the lack of measurement data by assuming sparsity of the material parameters in an arbitrary basis. Using measurements obtained from a wire and a multi-tissue phantom, we evaluate the performance of our CS solution in comparison to synthetic aperture focussing, delay-and-sum (DAS) beamforming and filtered backpropagation (FBP). Emitting only a single plane wave, the CS approach yields the best results for the sparse wire phantom in terms of sidelobe reduction and lateral -6 dB-widths. For the non-sparse multi-tissue phantom, we observe equivalent results for CS, DAS, and FBP when a single plane wave is emitted and a discrete cosine basis is employed as sparsifying transform.

I. INTRODUCTION

For real-time visualization of time-variant processes in diagnostic ultrasound imaging (e. g. heart motion, blood and contrast agent flow, trajectory of propagating shear waves) the acquisition time for a single image is crucial. This time depends on the number of sequentially emitted sound waves, the maximum penetration depth, as well as on the speed of sound in the investigated medium.

Established B-mode or synthetic aperture (SA) concepts usually utilize a large number of sequentially emitted sound waves (on the order of 64 – 512) to acquire a single image. They are thus relatively slow. Alternative concepts, like the emission of only few plane or spherical waves combined with delay-and-sum (DAS) beamforming or filtered backpropagation (FBP) [1], allow fast image acquisition, however, the resulting images often suffer from a degraded lateral resolution and reduced contrast in comparison to B-mode or SA images.

One major cause for these drawbacks is that the inverse scattering problem arising in pulse-echo imaging configurations is usually ill-posed. Measurements of the scattered sound caused by only few emitted sound waves are insufficient to reconstruct an arbitrary distribution of material parameters. This problem becomes even more significant in three-dimensional ultrasound imaging. For a high-quality reconstruction, additional constraints are necessary.

Recently, compressive sensing (CS) has been introduced as a concept for the fast acquisition of compressible noisy

This research is part of ForSaTum (<http://www.forsatum.de>) sponsored by Ziel2.NRW “Regionale Wettbewerbsfähigkeit und Beschäftigung” 2007 – 2013 co-financed by the European regional development fund (ERDF), grant no. 005-0908-0117.

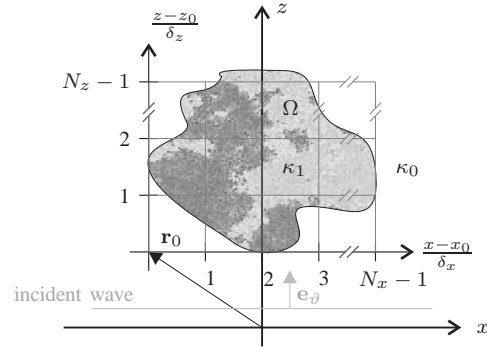


Fig. 1. Classical scan configuration employed in two-dimensional pulse-echo ultrasound imaging.

signals [2]. Assuming sparsity of the signal in a suitable basis, its aim is to reconstruct the signal from only few physical measurements. CS has been adopted in different medical imaging modalities, e. g. magnetic resonance imaging [3] and photoacoustic tomography [4]. While maintaining image quality, a significant reduction of the number of measurements and thus of acquisition time was achieved [3], [4].

In this contribution we investigate the performance of CS in fast pulse-echo ultrasound imaging. Although special emphasis will be laid on the experimental investigation of the two-dimensional imaging case, the established mathematical framework is valid for the three-dimensional case as well.

II. MATHEMATICAL FRAMEWORK

A. Solution To The Wave Equation For Inhomogeneous Media

The classical scan configuration employed in two-dimensional pulse-echo ultrasound imaging is illustrated in Fig. 1. An inhomogeneous medium (gray region) with compressibility κ_1 is surrounded by a homogeneous medium with constant compressibility κ_0 . The space occupied by the inhomogeneous medium is described by the set $\Omega \subset \mathbb{R}^n \setminus \{z \leq 0\}$, where $n \in \{2, 3\}$. For $\mathbf{r} \in \mathbb{R}^n$, compressibility κ is then given by

$$\kappa(\mathbf{r}) = \begin{cases} \kappa_1(\mathbf{r}) & \text{for } \mathbf{r} \in \Omega, \\ \kappa_0 & \text{for } \mathbf{r} \notin \Omega. \end{cases}$$

An incident sound wave propagating through the homogeneous medium is scattered within and at the boundary of the inhomogeneous medium Ω . Assuming monochromatic

perturbations with angular frequency ω the acoustic pressure p is governed by the equation [5]

$$(\Delta + k_0^2)p(\mathbf{r}) = m(\mathbf{r}), \quad (1)$$

where Δ denotes the Laplacian, $k_0 = \omega c_0^{-1}$ is the wavenumber, $c_0 = (\kappa_0 \rho_0)^{-1/2}$ is the small-signal sound speed in the homogeneous medium, ρ_0 is the constant mass density of both media and

$$m(\mathbf{r}) = k_0^2 \gamma_\kappa(\mathbf{r}) p(\mathbf{r}), \quad (2)$$

with the relative deviation $\gamma_\kappa(\mathbf{r}) = 1 - \kappa(\mathbf{r})\kappa_0^{-1}$. The acoustic pressure \tilde{p} in time domain is related to p via the identity

$$\tilde{p}(\mathbf{r}, t) = \text{Re} \{ p(\mathbf{r}) e^{j\omega t} \}.$$

Without loss of generality, the acoustic pressure $p = p_{\text{in}} + p_{\text{sc}}$ is assumed to be the sum of the incident acoustic pressure p_{in} and the scattered acoustic pressure p_{sc} in each point. The incident acoustic pressure satisfies the homogeneous Helmholtz equation and describes the sound field present without any medium inhomogeneities. The scattered acoustic pressure p_{sc} is solely caused by the inhomogeneous medium and satisfies the *Sommerfeld* radiation condition [5], [6]. The solution for the acoustic pressure p is then implicitly described by the *Lippmann-Schwinger* equation

$$p(\mathbf{r}) = p_{\text{in}}(\mathbf{r}) + k_0^2 \int_{\Omega} \gamma_\kappa(\mathbf{r}') p(\mathbf{r}') G(\mathbf{r} - \mathbf{r}') d\mathbf{r}', \quad (3)$$

where

$$G(\mathbf{r}) = \begin{cases} \frac{j}{4} H_0^{(2)}(k_0 \|\mathbf{r}\|_2) & \text{for } n = 2, \\ -\frac{1}{4\pi} \frac{e^{-jk_0 \|\mathbf{r}\|_2}}{\|\mathbf{r}\|_2} & \text{for } n = 3, \end{cases} \quad (4)$$

denotes the free space Green's function satisfying the radiation condition and

$$(\Delta + k_0^2)G(\mathbf{r}) = \delta(\mathbf{r}),$$

$\|\mathbf{r}\|_2$ is the L^2 norm of \mathbf{r} (*Euclidean* length), $H_0^{(2)}$ denotes the zero-order *Hankel* function of second kind and δ indicates the n -dimensional *Dirac* delta distribution.

B. Inverse Problem

In ultrasound imaging the goal is to reconstruct the parameter γ_κ within a specified field-of-view (FOV) from measurements of the scattered acoustic pressure p_{sc} at a finite number of discrete locations on the x -axis ($n = 2$) or on the plane $z = 0$ ($n = 3$). In this contribution we assume that γ_κ can be approximated by point scatterers located on a regular lattice. The spatial extent of the lattice determines the FOV. A similar approach was presented in [7] to solve an inverse scattering problem assuming plane wave far field conditions using CS.

Let $\mathbf{r}_0 = (x_0, z_0)^T \in \mathbb{R}^2 \setminus \{z \leq 0\}$ denote an arbitrary offset vector, \mathbf{e}_x and \mathbf{e}_z indicate the unit vectors in the direction of the positive coordinate axes, and let N_x , N_z , δ_x and δ_z be the number of lattice points as well as the spacing between adjacent lattice points on these axes. For $n = 2$, the lattice can then be defined as the set

$$\mathcal{L} = \{ \mathbf{r}_i \in \mathbb{R}^2 : \mathbf{r}_i = \mathbf{r}_0 + i_x \delta_x \mathbf{e}_x + i_z \delta_z \mathbf{e}_z, \\ 0 \leq i_x < N_x, 0 \leq i_z < N_z, i = i_x N_z + i_z \}.$$

The parameter γ_κ consequently becomes

$$\gamma_\kappa(\mathbf{r}) = \sum_{i=0}^{N-1} \gamma_{\kappa,i} \delta(\mathbf{r} - \mathbf{r}_i), \quad (5)$$

where $N = N_x N_z$ is the total number of lattice points. The lattice is illustrated in Fig. 1 for $n = 2$.

In pulse-echo ultrasound imaging both the acoustic pressure p and γ_κ in Ω are usually unknown. There exist different approximations in literature in order to reduce the number of unknowns in Ω to γ_κ , e.g. the *Born* or *Rytov* approximations [8]. In a first step, we employ the first Born approximation. The acoustic pressure p in the integral in (3) is replaced by the incident acoustic pressure p_{in} . For the sake of simplicity we assume plane wave excitation. Thus

$$p_{\text{in}}(\mathbf{r}, \mathbf{e}_\vartheta) = A_{\text{in}}(k_0) e^{-jk_0 \mathbf{e}_\vartheta \cdot \mathbf{r}}, \quad (6)$$

where \mathbf{e}_ϑ denotes the unit vector in the direction of propagation and A_{in} is the frequency-dependent complex-valued amplitude. Plugging (5) and (6) into (3) yields

$$p_{\text{sc}}(\mathbf{r}, \mathbf{e}_\vartheta) = k_0^2 A_{\text{in}}(k_0) \sum_{i=0}^{N-1} \gamma_{\kappa,i} e^{-jk_0 \mathbf{e}_\vartheta \cdot \mathbf{r}_i} G(\mathbf{r} - \mathbf{r}_i). \quad (7)$$

Assuming an $(n-1)$ -dimensional linear array transducer with N_{el} elements, the scattered acoustic pressure can be measured at equidistant discrete locations on the x -axis ($n = 2$) or on the plane $z = 0$ ($n = 3$). Let $\delta_{s,x}$ denote the spacing of the transducer elements on the x -axis. For $n = 2$, the measurement locations are elements of the set

$$\mathcal{M} = \left\{ \mathbf{r}_{m,l} \in \mathbb{R}^2 : \mathbf{r}_{m,l} = \left(l - \frac{N_{\text{el}} - 1}{2} \right) \delta_{s,x} \mathbf{e}_x, 0 \leq l < N_{\text{el}} \right\}.$$

Using vector-matrix notation, we define the $N_{\text{el}} \times 1$ vector

$$\mathbf{p}_{\text{sc}}(k_0, \mathbf{e}_\vartheta) = (p_{\text{sc}}(\mathbf{r}_{m,0}, \mathbf{e}_\vartheta), \dots, p_{\text{sc}}(\mathbf{r}_{m,N_{\text{el}}-1}, \mathbf{e}_\vartheta))^T,$$

the $N \times 1$ vector

$$\boldsymbol{\gamma}_\kappa = (\gamma_{\kappa,0}, \dots, \gamma_{\kappa,N-1})^T$$

as well as the $N_{\text{el}} \times N$ matrix

$$G_{l,i}(k_0, \mathbf{e}_\vartheta) = k_0^2 A_{\text{in}}(k_0) e^{-jk_0 \mathbf{e}_\vartheta \cdot \mathbf{r}_i} G(\mathbf{r}_{m,l} - \mathbf{r}_i).$$

For each wavenumber the identity

$$\mathbf{p}_{\text{sc}}(k_0, \mathbf{e}_\vartheta) = \mathbf{G}(k_0, \mathbf{e}_\vartheta) \boldsymbol{\gamma}_\kappa$$

holds. For broadband insonification with N_k different wavenumbers thus

$$\mathbf{p}_{\text{sc}}(\mathbf{e}_\vartheta) = \begin{pmatrix} \mathbf{G}(k_{0,0}, \mathbf{e}_\vartheta) \\ \vdots \\ \mathbf{G}(k_{0,N_k-1}, \mathbf{e}_\vartheta) \end{pmatrix} \boldsymbol{\gamma}_\kappa = \mathbf{G}(\mathbf{e}_\vartheta) \boldsymbol{\gamma}_\kappa, \quad (8)$$

where $\mathbf{G}(\mathbf{e}_\vartheta)$ is a complex-valued $N_{\text{el}} N_k \times N$ matrix.

The parameter $\boldsymbol{\gamma}_\kappa$ can then be recovered by solving the convex optimization problem [2]

$$\hat{\boldsymbol{\gamma}}_\kappa = \arg \min_{\mathbf{x} \in \mathbb{C}^N} \|\mathbf{x}\|_1 \quad \text{s. t.} \quad \|\mathbf{G}(\mathbf{e}_\vartheta) \mathbf{x} - \mathbf{p}_{\text{sc}}(\mathbf{e}_\vartheta)\|_2 \leq \epsilon, \quad (9)$$

where $\|\mathbf{x}\|_1 = \sum_{i=0}^{N-1} |x_i|$ is the L^1 norm of \mathbf{x} and ϵ is a measure for noise and inaccuracy of the physical model.

C. Implementation

The optimization problem (9) was solved using SPGL1 [9]. This algorithm requires efficient implementations of the so-called forward and backward operators. The forward operator is the multiplication with the matrix $\mathbf{G}(\mathbf{e}_\vartheta)$ in (8). The backward operator is the multiplication with the Hermitian conjugate $\mathbf{G}^H(\mathbf{e}_\vartheta)$. Implementing the respective matrix-vector multiplications requires careful memory allocation. For a problem of typical size, e.g. $N_x \approx 400$, $N_z \approx 600$, $N_{\text{el}} \approx 128$ and $N_k \approx 1000$, the memory occupied by the measurement matrix $\mathbf{G}(\mathbf{e}_\vartheta)$ is approx. 458 GB, assuming complex-valued arithmetic with 64 bit double precision. Consequently, the storage of all matrix elements in random access memory is impossible on standard PCs. Instead, each matrix element has to be recomputed during the matrix-vector multiplication. The necessary computations lend themselves for parallel processing. We employed a Tesla C2070 (NVIDIA Corp., Santa Clara, CA, USA) GPU computing processor with 32 bit single precision. For simplicity, the Hankel function in (4) was replaced by its asymptotic form [10]

$$H_0^{(2)}(k_0 \|\mathbf{r}\|_2) \approx \sqrt{\frac{2}{\pi k_0 \|\mathbf{r}\|_2}} e^{-j(k_0 \|\mathbf{r}\|_2 - \frac{\pi}{4})}$$

that is valid for $\|\mathbf{r}\|_2 \gg \lambda$.

III. EXPERIMENTAL VALIDATION

A. Experimental Setup

We acquired measurement data from two phantoms using a linear array transducer L14-5/38 ($N_{\text{el}} = 128$ elements) connected to a SonixTouch Research system (Ultrasonix Medical Corp., Richmond, BC, Canada). For both phantoms, full synthetic aperture (SA, cf. [11]) scans were performed. To enhance signal-to-noise ratio (SNR), we computed the average of 80 scans for each phantom and applied a digital band pass filter. The averaged and filtered SA data were used to compute a reference image for each phantom and to synthesize measurements that would have been obtained by plane wave excitation (6) with $\mathbf{e}_\vartheta = \mathbf{e}_z$.

Phantom A was employed to demonstrate the ability of our approach to reconstruct sparse parameters γ_κ . It consisted of four wires (diameter: 50 μm) immersed in a water reservoir. The wires were located at an axial distance between 43 mm and 53 mm from the transducer array. The lateral spacing between the wires was about 3 mm to 5 mm. The small-signal sound speed was assumed to be $c_0 = 1502 \text{ m s}^{-1}$.

Phantom B was a CIRS model 040 multi-purpose ultrasound phantom (Computerized Imaging Reference Systems, Norfolk, Virginia, USA). The phantom was used to investigate the ability of our approach to recover non-sparse parameters γ_κ and to handle attenuation ($0.5 \text{ dB MHz}^{-1} \text{ cm}^{-1}$). We used a discrete cosine transform to sparsify γ_κ . Small-signal sound speed was assumed to be $c_0 = 1540 \text{ m s}^{-1}$.

In order to compare the presented approach to existing concepts, a delay-and-sum (DAS) algorithm adapted to the

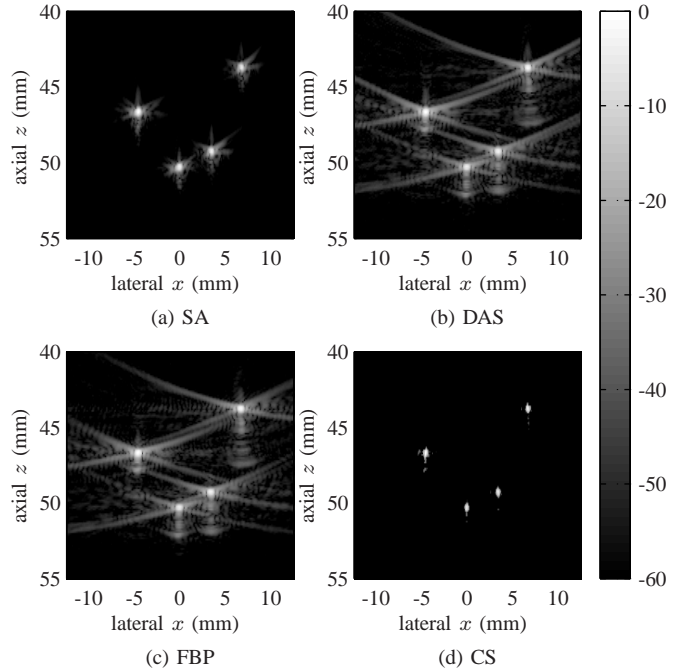


Fig. 2. Images obtained from phantom A (four wires, diameter: 50 μm) for (a) full SA approach, (b) DAS, (c) FBP, and (d) CS. In (a) $N_{\text{el}} = 128$ single element emissions were used while in (b), (c), and (d) only a single plane wave was emitted. Parameters were: $N_x = 401$, $N_z = 601$, $N_k = 1008$, $\delta_x = \delta_z = 100 \mu\text{m}$ (except for FBP, $\delta_x = 101.6 \mu\text{m}$), $\mathbf{e}_\vartheta = \mathbf{e}_z$, $\epsilon = 0.2 \|\mathbf{p}_{\text{sc}}(\mathbf{e}_\vartheta)\|_2$. All values are in dB.

excitation with plane waves as well as a filtered backpropagation (FBP) procedure (see [1] for details) were investigated besides SA. As the presented approach, both algorithms use measurement data obtained by a single plane wave emission (6) and thus lend themselves for fast imaging. The unknown spectrum A_{in} in (6) was assumed constant with a linear phase. In practice, it depends on the exact transfer function of the transducer array and the excitation voltage.

B. Experimental Results

Details of the images obtained from phantom A are shown in Fig. 2 for all four reconstruction procedures. The recovered images using DAS (b) and FBP (c) suffer from strong sidelobe artifacts due to the missing transmit focussing. These are reduced in the SA approach (a) by increasing the number of sequential wave emissions, and thus by introducing transmit focussing retrospectively. Although only one plane wave emission is employed, the presented CS approach (d) eliminates sidelobes completely. Fig. 3 displays the axial (a) and lateral (b) image profiles obtained by summing the absolute values along each axis. Obviously, DAS (dash-dotted) and FBP (dotted) as well as SA (dashed) and CS (solid) yield similar axial -6 dB-widths (also solid). The lateral -6 dB-widths of CS are clearly smaller than those achieved by SA, DAS and FBP.

Details of the images obtained from phantom B are shown in Fig. 4. In contrast to phantom A, sidelobe artifacts are not visible. The wires in (b) and (c) exhibit a similar lateral

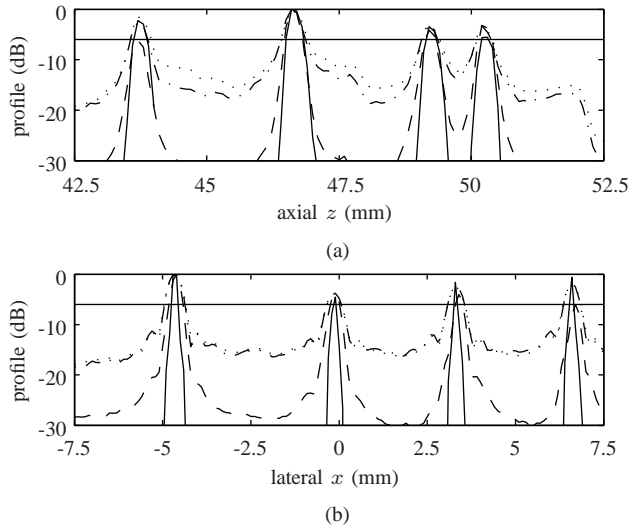


Fig. 3. Axial (a) and lateral (b) image profiles obtained from phantom A for all four reconstruction procedures. Legend: SA (dashed), DAS (dash-dotted), FBP (dotted), CS (solid), -6 dB-line (also solid)

extent. This extent is slightly larger in (d). Hyperechoic and anechoic regions are clearly visible in (b) and (d). The finite aperture causes the FBP image (c) to become gradually darker with increasing axial distance. Thus, the anechoic region at $z = 40$ mm is barely visible.

IV. CONCLUSION

We investigated the performance of CS in solving the inverse scattering problem arising in pulse-echo diagnostic ultrasound imaging. For sparse parameters γ_{κ} CS yields the best solutions to the inverse scattering problem in terms of sidelobe reduction and lateral -6 dB-widths. It even outperforms the SA approach, although the number of sequential wave emissions is significantly reduced from N_{el} single element emissions to a single plane wave emission. According to these results, CS lends itself for fast ultrasound imaging of sparse objects. For non-sparse parameters γ_{κ} the results obtained by our current implementation of the CS approach are similar to those obtained by DAS and FBP. They can probably be improved by finding a more suitable sparsifying basis for ultrasound images.

REFERENCES

[1] M. F. Schiffner and G. Schmitz, "Plane Wave Pulse-Echo Ultrasound Diffraction Tomography With A Fixed Linear Transducer Array," in *Proceedings of the 31st International Symposium on Acoustical Imaging*, April 2011, in press.
 [2] E. J. Candès and M. B. Wakin, "An Introduction To Compressive Sampling," *IEEE Signal Processing Magazine*, vol. 25, no. 2, pp. 21–30, March 2008.

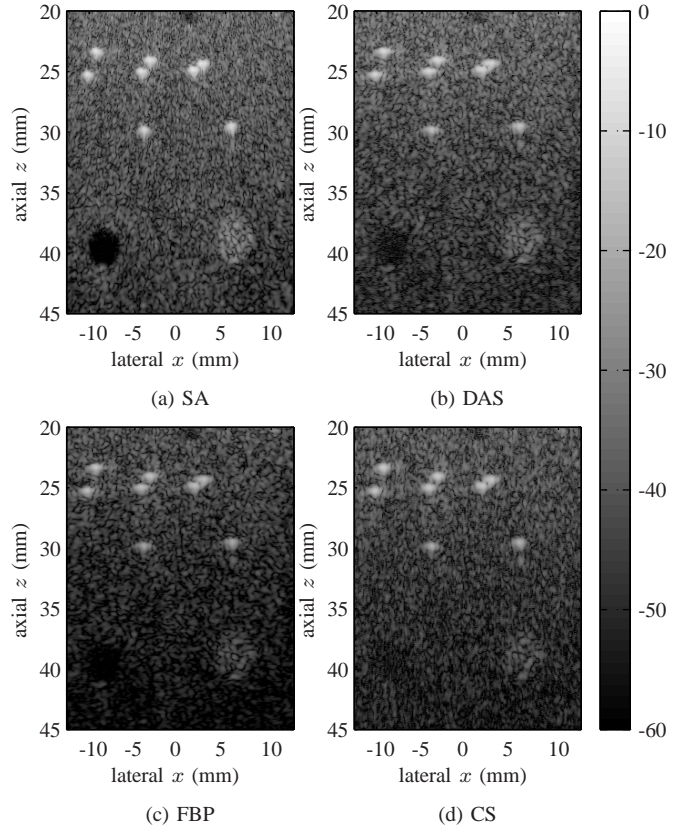


Fig. 4. Images obtained from phantom B (CIRS 040) for (a) full SA approach, (b) DAS, (c) FBP, and (d) CS. In (a) $N_{el} = 128$ single element emissions were used while in (b), (c), and (d) only a single plane wave was emitted. Parameters were: $N_x = 401$, $N_z = 1001$, $N_k = 887$, $\delta_x = 100 \mu\text{m}$, $\delta_z = 60 \mu\text{m}$, (except for FBP, $\delta_x = 101.6 \mu\text{m}$), $\mathbf{e}_{\theta} = \mathbf{e}_z$, $\epsilon = 0.2 \|\mathbf{p}_{sc}(\mathbf{e}_{\theta})\|_2$. All values are in dB.

[3] M. Lustig, D. Donoho, and J. M. Pauly, "Sparse MRI: The application of compressed sensing for rapid MR imaging," *Magnetic Resonance in Medicine*, vol. 58, no. 6, pp. 1182–1195, December 2007.
 [4] Z. Guo, C. Li, L. Song, and L. V. Wang, "Compressed sensing in photoacoustic tomography in vivo," *Journal of Biomedical Optics*, vol. 15, no. 2, pp. 021 311–1–021 311–6, March/April 2010.
 [5] A. D. Pierce, *Acoustics - An Introduction to Its Physical Principles and Applications*. Acoustical Society of America, 1989.
 [6] F. Natterer and F. Wübbeling, *Mathematical Methods in Image Reconstruction*. Philadelphia: Society for Industrial and Applied Mathematics (SIAM), 2001.
 [7] A. C. Fannjiang, "Compressive inverse scattering: II. Multi-shot SISO measurements with born scatterers," *Inverse Problems*, vol. 26, no. 3, 2010.
 [8] J. M. Blackledge, *Digital Image Processing - Mathematical and Computational Methods*. Chichester: Horwood Publishing, 2005.
 [9] E. van den Berg and M. P. Friedlander, "Probing the pareto frontier for basis pursuit solutions," *Journal of Scientific Computing*, vol. 31, no. 2, pp. 890–912, 2008.
 [10] M. Abramowitz and I. A. Stegun, Eds., *Handbook of Mathematical Functions With Formulas, Graphs and Mathematical Tables*, 10th ed. National Bureau of Standards, 1972.
 [11] J. A. Jensen, S. I. Nikolov, K. L. Gammelmark, and M. H. Pedersen, "Synthetic aperture ultrasound imaging," *Ultrasonics*, vol. 44, pp. e5–e15, December 2006.